Journal of Alloys and Compounds 507 (2010) 245–252

Contents lists available at ScienceDirect

Journal of Alloys and Compounds

journal homepage: www.elsevier.com/locate/jallcom

Template-free synthesis, growth mechanism and photoluminescent properties of $Ln(OH)_3$ and Ln_2O_3 nanorods (Ln: lanthanide ion)

Tian Xia[a,*], Jingping Wang[b], Nan Lin[a], Lihua Huo[a], Hui Zhao[a], Grigoris Mountrichas[c]

[a] Key Laboratory of Functional Inorganic Materials Chemistry, Ministry of Education, School of Chemistry, Chemical Engineering and Materials, Heilongjiang University, Harbin 150080, Heilongjiang, People's Republic of China
[b] College of Materials Science and Chemical Engineering, Harbin Engineering University, Harbin 150001, Heilongjiang, People's Republic of China
[c] Theoretical and Physical Chemistry Institute, National Hellenic Research Foundation, Athens 11635, Greece

ARTICLE INFO

Article history:
Received 16 June 2009
Received in revised form 22 July 2010
Accepted 27 July 2010
Available online 4 August 2010

Keywords:
Nanostructured materials
Crystal growth
Optical properties
Scanning electron microscopy (SEM)

ABSTRACT

Uniform and well-defined single-crystalline $Ln(OH)_3$ and $La(OH)_3$:Eu^{3+} (Ln: lanthanide ion) nanorods were successfully synthesized by a large-scale and facile hydrothermal method only using $Ln(NO_3)_3 \cdot 6H_2O$ as lanthanide source and H_2O_2 as controller without any surfactant or template. The as-formed product via the hydrothermal process, $La(OH)_3$:Eu^{3+}, could transform to hexagonal La_2O_3:Eu^{3+} with the same morphology by a postannealing process. The above mentioned samples were characterized by means of X-ray diffraction (XRD), field-emission scanning electron microscopy (FE-SEM), transmission electron microscopy (TEM), high-resolution transmission electron microscopy (HRTEM), selected area electron diffraction (SAED) and photoluminescence (PL) spectra. By tuning the hydrothermal treatment time, a morphological evolution between the nanoparticles and nanorods was observed. Furthermore the growth mechanism and the morphological evolution of different shapes were investigated. Unlike traditional synthesis of $Ln(OH)_3$, H_2O_2 does not leave any impurity in the reaction system and makes the process very simple to obtain and separate the nanoparticles, nanomultipods and nanorods morphology. The La_2O_3:Eu^{3+} nanorods exhibit a strong red emission corresponding to $^5D_0 \rightarrow {}^7F_2$ transition (625 nm) of Eu^{3+} under UV light excitation (282 nm), which have potential applications in fluorescent devices.

1. Introduction

In modern chemistry and materials science, one-dimensional (1D) nanostructures, including nanorods, nanotubes, nanowires, nanobelts and nanofibers, have attracted much interest because of the interrelation between the properties of the materials and the geometrical characteristics of the structures, such as shape, dimensionality and size [1,2]. Novel applications could be developed as a result of shape-controllable nanocrystals synthesis. So far many efforts have been devoted to develop new methods for the preparation of high quality inorganic nanostructures, which could open a new domain of chemical and technological interest.

As a well-known inorganic functional material, rare earth compounds, such as hydroxides [3–5], oxides [6–8], phosphates [9,10], vanadates [11,12], borates [13,14], fluorides and sulfides [15–17], have been extensively studied because of their large potential applications in high-performance luminescent and magnetoresistance devices, catalysts and electrodes because of their outstanding optical, electrical and magnetic properties arising from their unique electronic structures, which involve 4f electrons. However, dimensionality and morphology are now considered to be the particularly important factors that could influence the chemical and physical properties of the synthesized materials. The use of rare earth compounds, in the form of 1D nanocrystals, with controllable morphology, could lead to the high quality materials due to both the shape-specific nature of the material and the quantum effects. From the application point of view, nanomaterials should not only be synthesized in a shape-controllable way, having the desired composition, reproduced morphology, size and structure but also be prepared using simple and environmentally friendly methodologies. The most widely used approach for the synthesis of 1D nanostructures is the template or catalyst-based synthesis in which catalysts act as the energetically preferential sites for the reactant molecules while the templates are used to confine the growth of the 1D nanocrystals. Recent studies suggest that the 1D nanostructure might be prepared under properly controlled condition without the presence of catalysts or templates [18,19]. The above mentioned preparation implies that the formation of the 1D nanostructure is thermodynamically preferable for many substances under certain conditions. As we know, environmentally friendly synthetic methodologies that include template synthesis, molten-salt synthesis, and hydrothermal processing have gradually been

* Corresponding author. Tel.: +86 451 86608426; fax: +86 451 86608040.
E-mail address: xiatian0621@yahoo.com.cn (T. Xia).

0925-8388/$ – see front matter © 2010 Elsevier B.V. All rights reserved.
doi:10.1016/j.jallcom.2010.07.169

Table 1
Summary of the experimental conditions and morphological properties of the final samples.

Sample	T (°C)	Time (h)	Ln source	Additive	Phase and morphology (size, aspect ratio)
P1	150	24	$La(NO_3)_3$	H_2O_2	$La(OH)_3$ nanorods (15 nm × 400 nm; 26)
P2	150	24	$Nd(NO_3)_3$	H_2O_2	$Nd(OH)_3$ nanorods (15 nm × 400 nm; 26)
P3	150	24	$Sm(NO_3)_3$	H_2O_2	$Sm(OH)_3$ nanorods (15 nm × 400 nm; 26)
P4	150	24	$Eu(NO_3)_3$	H_2O_2	$Eu(OH)_3$ nanorods (15 nm × 400 nm; 26)
P5	150	24	$La(NO_3)_3$ $Eu(NO_3)_3$	H_2O_2	$La(OH)_3$:Eu^{3+} nanorods (20 nm × 200 nm; 10)
P6	800	6	P5	No	La_2O_3:Eu^{3+} nanorods (15 nm × 200 nm; 13)
P7	150	24	$La(NO_3)_3$	No	$La(OH)_3$ nanodisks (10 nm in thickness, 200 nm)
P8	150	1	$La(NO_3)_3$	H_2O_2	$La(OH)_3$ nanospheres (15 nm)
P9	150	6	$La(NO_3)_3$	H_2O_2	$La(OH)_3$ nanospheres (15 nm) and nanomultipods (pods: 15 nm × 200 nm; 10)
P10	150	12	$La(NO_3)_3$	H_2O_2	$La(OH)_3$ nanorods (15 nm × 300 nm; 20)

implemented as effective techniques in the preparation of nanostructures. Especially the hydrothermal synthesis technique is an important method for the preparation of low-dimensional nanomaterials keeping all the advantages of high quality, purity and good homogeneity. The environmental friendly character of the above method is explained from the fact that neither template nor catalyst is required. It is well-known that 1D rare earth hydroxides are usually obtained through hydrothermal treatment of their counterpart oxides, using acid and base. Li's and Yada's groups opened up the possibility of a general method for 1D $Ln(OH)_3$ nanostructures via the hydrothermal process [20,21]. Up to now, there are many reports about 1D lanthanide hydroxides and oxides prepared by the hydrothermal method and postcalcining process [8,22–25]. Among them, lanthanum hydroxides [$La(OH)_3$] have been used as the catalysts and sorbents, and the precursors for the preparation of oxides and sulfides by thermal dehydration and sulfurization, respectively. The Eu^{3+}-dpoped La_2O_3 is one of the important red-emitting phosphors. Although the La_2O_3:Eu^{3+} phosphors have been extensively studied, few studies have been presented for the synthesis of separated, uniform and well-defined 1D La_2O_3:Eu^{3+} nanostructures and its luminescent properties.

Herein, we report a large-scale and facile hydrothermal synthesis method of uniform and well-defined 1D lanthanide hydroxide nanorods, and the preparation of La_2O_3:Eu^{3+} nanorods through a subsequent heat treatment process without using any catalyst, template and surfactant. The growth mechanism of the lanthanide hydroxide nanorods is investigated in detail. Moreover, the photoluminescent properties of the nanostructures are presented under the prism of a high-performance phosphor application.

2. Experimental details

$Ln(OH)_3$ (Ln = La, Nd, Sm and Eu) nanorods were synthesized by a simple hydrothermal process. In a typical synthesis, 2 g $Ln(NO_3)_3{\cdot}6H_2O$ (both with purity of 99.99%, Tianjin Delan Fine Chemical Company, China) was dissolved in deionized water with agitation to form a clear solution, and 15 mL H_2O_2 solution (30 wt% Beijing Fine Chemical Company, China) was then added into this solution. Following 1 mol L^{-1} of NaOH solution was introduced dropwise to the vigorously stirred solution until pH = 11–12. After additional agitation for 1 h, the as-obtained colloidal precipitate was transferred to a 50 mL autoclave, sealed and heated at 150 °C for 24 h. The autoclave was then left to cool-down to room temperature. The precursors were recovered by filtration, washed with deionized water and ethanol several times, and dried at 60 °C in air for 24 h. In addition, $La(OH)_3$:Eu^{3+} was prepared with 19:1 molar ratio of $La(NO_3)_3$/$Eu(NO_3)_3$, having the same conditions as those for synthesizing $Ln(OH)_3$. It should be noted that all samples were hydrothermally treated at 150 °C for 24 h. The final products were retrieved through a heat treatment at 800 °C in air for 6 h with a heating rate of 1 °C min^{-1}. The detailed experimental parameters together with the morphological properties of the corresponding products (denoted as P1–P10) are listed in Table 1. The La_2O_3: 5 mol% Eu^{3+} bulk material was prepared by the conventional solid-state reaction. Stoichiometric amounts of La_2O_3 and Eu_2O_3 powders were mixed and ground in an agate motor, then calcined at 1000 °C for 24 h. The XRD pattern showed that a pure La_2O_3 phase was obtained.

The phase purity and crystallinity of the products were examined by powder X-ray diffraction (XRD) performed on a Rigaku-Dmax 2500 diffractometer with Cu Kα radiation (λ = 0.15405 nm) and a scanning rate of 2° min^{-1}. The operation voltage and current were maintained at 40 kV and 200 mA. The lattice parameters were calculated by the Rietveld analysis of the XRD data using the GSAS program. The transmission electron microscopy (TEM), high-resolution transmission electron microscopy (HRTEM) and the selected area electron diffraction (SAED) were taken with a JEOL-JEM-2010 operating at 200 kV (JEOL, Japan). Samples for TEM observation were prepared by dropping diluted suspension of the sample powder onto a standard carbon-coated (20–30 nm) Formvar film on a copper grid (230 mesh). The field-emission scanning electron microscopy (FE-SEM, XL-30, Philips) equipped with energy-dispersive spectrometer (EDS) was used to investigate the morphology and composition of samples. For SEM observation, the product was pasted on the silicon substrate. Photoluminescence (PL) excitation and emission spectra were recorded with a Hitachi F-4500 spectrophotometer equipped with a 150 W Xenon lamp as the excitation source. The operation parameters of PL test are the following: scan speed = 240 nm min^{-1}, delay = 0 s, EX slit = 2.5 nm, EM slit = 2.5 nm, and PMT voltage = 700 V. All the measurements were performed at room temperature.

3. Results and discussion

Fig. 1 shows the XRD patterns of the $Ln(OH)_3$ products (Ln = La, Nd, Sm and Eu) through the hydrothermal process. All diffraction peaks of the as-formed samples can be readily indexed to pure hexagonal of $Ln(OH)_3$ [space group: $P63/m$ (176)]. For example, the diffraction peaks of $Eu(OH)_3$ can be indexed to hexagonal-phase $Eu(OH)_3$ according to the Joint Committee on Powder Diffraction Standards (JCPDS) file no. 17-0781. The lattice parameters are calculated to be a = 0.6359(2) nm and c = 0.3637(7) nm by the Rietveld analysis of the XRD data. The refined lattice and profile parameters of $Ln(OH)_3$ are listed in Table 2.

The SEM images provide the direct information about the size and typical shapes of the as-prepared samples. Fig. 2 shows some representative SEM images of $Ln(OH)_3$ through the hydrothermal process. All the products are composed of a great deal of nanorods with a uniform size of about 400 nm in length and 15 nm in diameter. This suggests the high yield and good uniformity achieved with this method. The SEM images show clearly that the products

Table 2
Refined lattice and profile parameters of lanthanide hydroxides nanorods at room temperature.

Lanthanide hydroxides	Symmetry	Lattice parameters		Space group	*R*-factor	
		a (nm)	*c* (nm)		R_{wp}	R_p
$La(OH)_3$	Hexagonal	0.6545(1)	0.3858(6)	*P*63/*m*	13.45%	9.60%
$Nd(OH)_3$	Hexagonal	0.6432(7)	0.3742(4)	*P*63/*m*	8.91%	4.15%
$Sm(OH)_3$	Hexagonal	0.6385(8)	0.3739(5)	*P*63/*m*	6.16%	2.79%
$Eu(OH)_3$	Hexagonal	0.6359(2)	0.3637(7)	*P*63/*m*	7.54%	3.36%
$La(OH)_3$:5%Eu^{3+}	Hexagonal	0.6475(6)	0.3803(9)	*P*63/*m*	11.47%	8.74%
La_2O_3:5%Eu^{3+}	Hexagonal	0.3865(4)	0.6062(6)	*P*-3*m*1	8.29%	5.36%

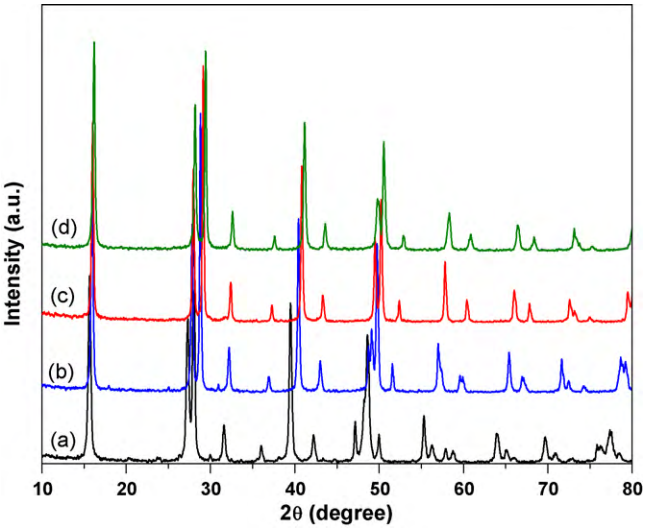

Fig. 1. XRD patterns of lanthanide hydroxide hydrothermally treated at 150 °C for 24 h: (a) $La(OH)_3$, (b) $Nd(OH)_3$, (c) $Sm(OH)_3$ and (d) $Eu(OH)_3$.

are cylindrical nanorods with smooth and flat surfaces while they have round ends. To examine carefully the lanthanide hydroxide nanostructures, the TEM observations were also performed. Images from TEM, HRTEM and SAED patterns of a typical $Nd(OH)_3$ nanorod are illustrated in Fig. 3. As shown in low-magnification TEM image (Fig. 3a), the as-obtained $Nd(OH)_3$ nanoparticles possess the perfect rodlike morphology with well-defined edges. Fig. 3b shows the HRTEM image of an individual nanorod recorded along the [0 0 1] direction. It can be seen that the corresponding (1 1 0) plane is oriented parallel to the nanorod growth direction (the *c*-axis) due to the resolved interplanar distance $d(1\,1\,0) = 0.319$ nm; the nanorods grow along the [0 0 1] direction (the *c*-axis). The corresponding SAED patterns (Fig. 3c) can be assigned to hexagonal $Nd(OH)_3$, indicating that the nanorod is a single-crystalline with its [1 0 0] orientation parallel to the electron beam. The HRTEM and SAED images of other lanthanide hydroxide nanorods are similar to those of $Nd(OH)_3$ nanorods.

Here, we select 5 mol% Eu^{3+} as doping ion to investigate the structures, morphologies and luminescent properties of $La(OH)_3$:Eu^{3+} and La_2O_3:Eu^{3+}. The XRD patterns of $La(OH)_3$:Eu^{3+} hydrothermally treated at 150 °C for 24 h are shown in Fig. 4a. No additional peaks of other phases are found, indicating that Eu^{3+} has been effectively introduced into the $La(OH)_3$ host lattice. The calculated lattice parameters, $a = 0.6475(6)$ nm and $c = 0.3803(9)$ nm, are well compatible with those values ($a = 0.6528$ nm and $c = 0.3855$ nm) from the standard card (JCPDS: 06-0585). It is noted that in the XRD patterns of $La(OH)_3$:Eu^{3+} the peak of (1 1 0) plane is strengthened greatly, which implies the anisotropic growth along identical orientation (*c*-axis). Fig. 5 presents the SEM, TEM, HRTEM micrographs and the SAED pattern of $La(OH)_3$:Eu^{3+} nanorod. As shown in SEM micrographs (Fig. 5a) and TEM image (Fig. 5b), the as-prepared $La(OH)_3$:Eu^{3+} nanoparticles are entirely composed of relatively uniform nanorods with length of 200 nm and diameter of about 20 nm. A HRTEM image of an individual nanorod (Fig. 5c) provides that the resolved lattice planes indicate a high degree of crystallinity. The interplanar distance is about 0.328 nm, close to the [1 1 0] lattice spacing of the hexagonal phase. The corresponding SAED pattern (Fig. 5d) recorded perpendicular to the growth axis of single nanorod can

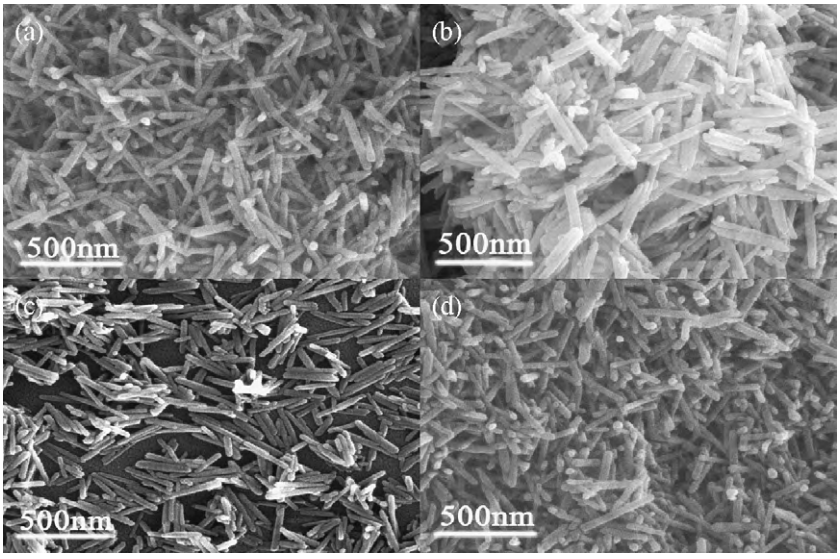

Fig. 2. FE-SEM images of lanthanide hydroxides hydrothermally treated at 150 °C for 24 h: (a) $La(OH)_3$, (b) $Nd(OH)_3$, (c) $Sm(OH)_3$ and (d) $Eu(OH)_3$.

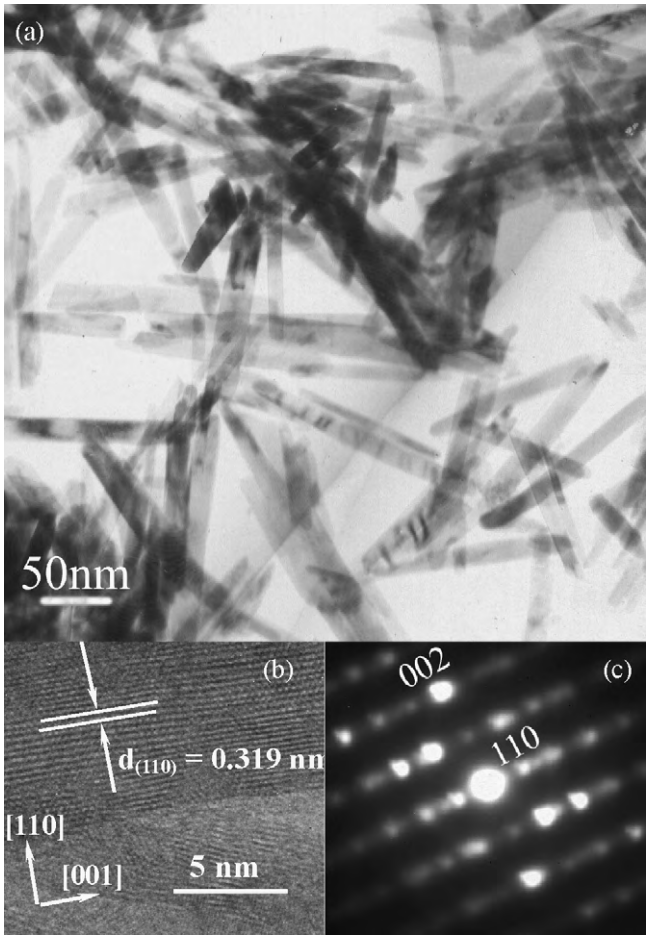

Fig. 3. (a) Low-magnification TEM image of $Nd(OH)_3$ hydrothermally treated at 150 °C for 24 h, (b) HRTEM image and (c) SAED pattern of a part of an individual $Nd(OH)_3$ nanorod.

be attributed to the [1 1 0] zone axis diffraction of hexagonal $La(OH)_3$:Eu^{3+}, suggesting that nanorod is a single-crystalline and grows along the [0 0 1] direction.

After the subsequent heat treatment, the hexagonal $La(OH)_3$:Eu^{3+} transforms into hexagonal La_2O_3:Eu^{3+}, as identified in Fig. 4b. All diffraction peaks can be readily indexed to the pure hexagonal phase of La_2O_3 [space group: *P*-3*m*1(164)] according to the JCPDS file no. 05-0602. No additional peaks of other phases have been detected, indicating that Eu^{3+} has been effectively introduced into the La_2O_3 host lattice. The lattice parameters of the calcined products were calculated to be $a = 0.3865(4)$ nm and $c = 0.6062(6)$ nm, which are lower than those of La_2O_3 ($a = 0.3937$ nm and $c = 0.6130$ nm, JCPDS: 05-0602) reflecting the incorporation of a smaller number of Eu^{3+} in the lattice. The refined lattice and profile parameters of $La(OH)_3$: 5%Eu^{3+} and La_2O_3: 5%Eu^{3+} nanorods are listed in Table 2. Fig. 5e shows the typical SEM images of La_2O_3:Eu^{3+} nanorods. It is noted that the La_2O_3:Eu^{3+} products inherit the rodlike morphology, but their size is slightly shrunk in comparison with the $La(OH)_3$:Eu^{3+} nanorods, while the density of the former nanorods is higher than that of the latter. $La(OH)_3$:Eu^{3+} nanorods were converted to La_2O_3:Eu^{3+} during the subsequent calcination process with gradual elimination of H_2O. Nevertheless, the conversion did not result any change in the morphology. Fig. 5f exhibits a typical low-magnification TEM image of La_2O_3:Eu^{3+} nanorods. It is found that the La_2O_3:Eu^{3+} nanorods are also smooth and uniform. Fig. 5g is the HRTEM image with a clearly revolved interplanar distance $d(1\,0\,0) = 0.336$ nm. The (1 0 0) planes are oriented vertical to the nanorod growth axis. The corresponding SAED pattern (Fig. 5h) taken from an individual nanorod can be indexed as the (1 0 0), (0 0 2), (1 0 1), and (1 0 2) reflections of the hexagonal La_2O_3, in agreement with the XRD results.

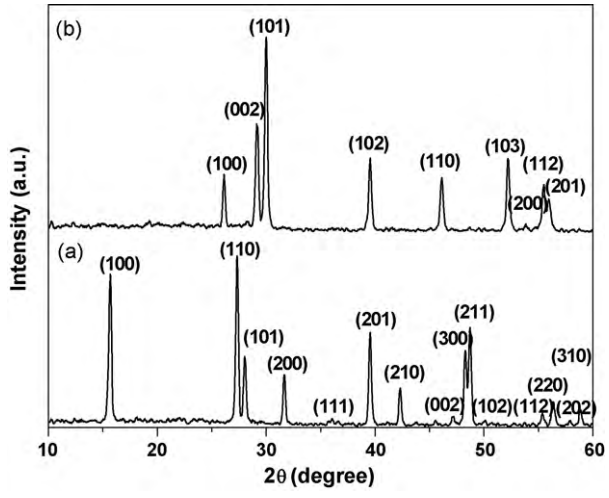

Fig. 4. (a) XRD pattern of the hydrothermal product $La(OH)_3$:Eu^{3+} nanorods, (b) XRD pattern of La_2O_3:Eu^{3+} nanorods obtained by calcining the as-prepared $La(OH)_3$:Eu^{3+} at 800 °C.

The luminescent properties of La_2O_3 nanorods doped with 5 mol% Eu^{3+} ions were investigated. The La_2O_3:Eu^{3+} nanorods exhibit a strong red emission under UV irradiation. The room-temperature photoluminescence (PL) excitation (a) and emission (b) spectra of the resulting La_2O_3:Eu^{3+} nanorod phosphors are presented in Fig. 6. The excitation spectrum was obtained by monitoring the emission of the Eu^{3+} $5D_0 \rightarrow 7F_2$ transition (625 nm), indicating that the Eu^{3+} ions prefer to hold a low symmetry site in the host material La_2O_3 [26]. It can be seen clearly that the excitation spectrum (Fig. 6a) consists of two broad bands with the maxima at 228 nm and 282 nm, which are attributed to the La_2O_3 host excitation band and the charge-transfer band (CTB) between O^{2-} and Eu^{3+}, respectively [26]. The presence of the La_2O_3 host excitation band in the excitation spectrum of Eu^{3+} indicates that there exists an energy transfer from the La_2O_3 host and La^{3+} to the doped Eu^{3+}. In the longer wavelength region, the f–f transition lines of Eu^{3+} (assigned in Fig. 6a) can be observed, even if they have very weak intensity compared with the CTB of O^{2-}-Eu^{3+}. Upon excitation into the CTB of Eu^{3+} at 282 nm, the obtained emission spectrum is composed of $^5D_{0,1,2} \rightarrow {}^7F_J$ ($J = 0, 1, 2, 3, 4$) transition lines of Eu^{3+} (Fig. 8B). Among all these transition lines of Eu^{3+}, the hypersensitive transition (625 nm) is the most prominent group. However, all the other emission peaks at 467 nm ($^5D_2 \rightarrow {}^7F_0$), 539 nm ($^5D_1 \rightarrow {}^7F_1$), 554 nm ($^5D_1 \rightarrow {}^7F_2$), 587, 595 nm ($^5D_0 \rightarrow {}^7F_1$), 651 nm ($^5D_0 \rightarrow {}^7F_3$), and 705 nm ($^5D_0 \rightarrow {}^7F_4$) have also been assigned in Fig. 6b. The presence of emission lines from higher excited states of Eu^{3+} ($^5D_1$, $^5D_2$) is attributed to the low vibration energy of the La–O band (500 cm^{-1}). The multiphoton relaxation by La–O vibration is not able to bridge the gaps between the higher energy levels ($^5D_1$, $^5D_2$) and the $^5D_0$ level of Eu^{3+} completely, leading to the emission from these levels [27]. The surface defects in nanocrystals should be highly increased compared to those in bulk materials. One can consider that in La_2O_3:Eu^{3+} nanorods, most of the exciton energies are transferred to the surface defects instead of Eu^{3+} ions, causing the intensity of the Eu^{3+} exciton band to decrease. However, the La_2O_3:Eu^{3+} nanorods show a strong red emission under UV light excitation, indicating that there are few surface defects in the prepared La_2O_3:Eu^{3+} nanorods [28]. In addition, the luminescence intensity is also related to the Eu–O bond distance [29]. Namely,

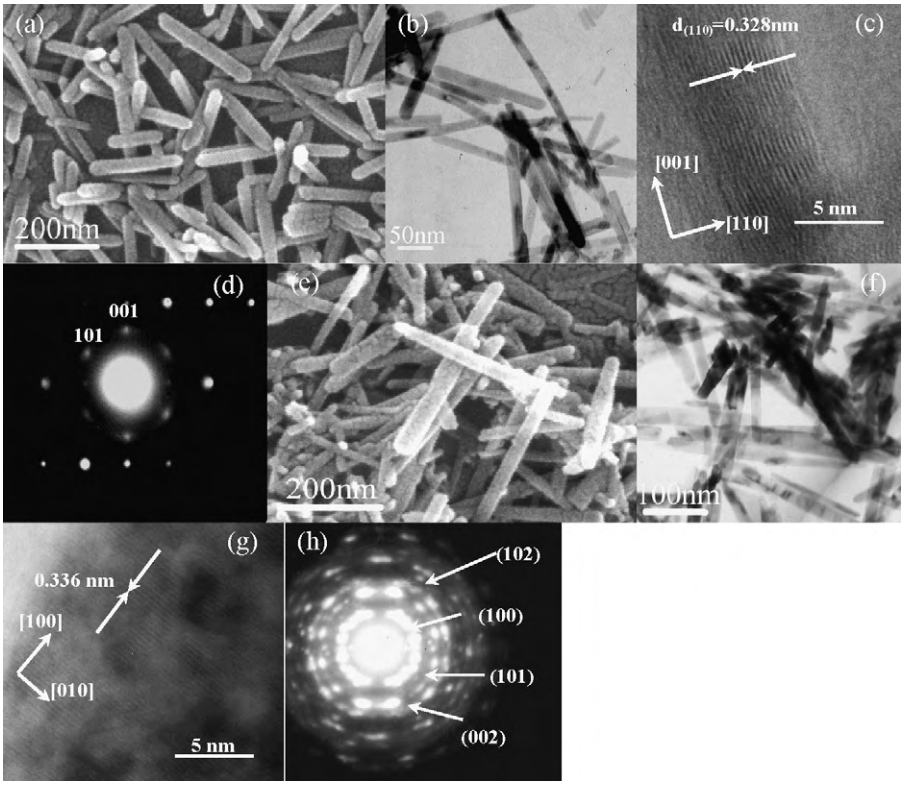

Fig. 5. (a) FE-SEM images of $La(OH)_3$:Eu^{3+} nanorods, (b) TEM images of $La(OH)_3$:Eu^{3+} nanorods, (c) HRTEM image and (d) SAED pattern of a part of an individual $La(OH)_3$:Eu^{3+} nanorod, (e) FE-SEM images of La_2O_3:Eu^{3+} nanorods, (f) TEM images of La_2O_3:Eu^{3+} nanorods, (g) HRTEM image and (h) SAED pattern of a part of an individual La_2O_3:Eu^{3+} nanorod.

the luminescence intensity is proportional to CTB. This result is in agreement with our experiments.

A comparison of emission spectra of the La_2O_3:Eu^{3+} nanorods sample with that of a bulk La_2O_3:Eu^{3+} sample under the same excitation condition is shown in Fig. 7. (Here it should be mentioned that all the experimental conditions were kept identical to avoid the experimental errors.) It can be seen that the La_2O_3:Eu^{3+} nanorods sample has a higher luminescence intensity compared to that of bulk one. Moreover, the relative intensity of the two peaks of $^5D_0 \rightarrow {}^7F_2$, located at 625 nm and 627 nm, is dramatically different in nanorod and bulk samples. In nanorods, the relative intensity of 625 nm peak increases a lot. This could be attributed to the different local environments around Eu^{3+} luminescence centers. More detailed experimental work is still in progress. Similar results have also been obtained by H.W. Song [30]. The increase in luminescence brightness for La_2O_3:Eu^{3+} nanorods sample indicates a potential application in phosphors fields.

A series of carefully designed experiments demonstrates that the shape evolution of $Ln(OH)_3$ nanocrystals is influenced by external factors such as the inorganic additives in the initial solution and reaction period with the intrinsic crystallographic structure of $Ln(OH)_3$ crystals.

One important factor for the adopted shape of the nanocrystals is the crystallographic phase of the initial seed. If the crystalline phase forms, the intrinsic structures of the seeds strongly affect the further crystal growth. In our experiments, it is noted that all samples experience a morphology transformation process during the crystal growth. In order to study the shape evolution of $Ln(OH)_3$ crystals, taking $La(OH)_3$ as an example, the detailed formation process of $La(OH)_3$ nanostructures was investigated by FE-SEM, and a clear time-dependent experiment was carried out under similar reaction conditions for synthesizing $La(OH)_3$. The corresponding XRD patterns and the SEM images of the intermediates obtained at different reaction time intervals are shown in Figs. 8 and 9, respectively. These results reveal that the intermediates show the different XRD patterns and morphologies at different reaction stages. The hydrothermal treatment for 1 h leads to the formation of (1 1 0) plane of pure hexagonal $La(OH)_3$ phase (Fig. 8a). A corresponding typical SEM image shows that $La(OH)_3$ products are composed of unique spherical nanoparticles with a mean diameter of 15 nm, as shown in Fig. 9a. In the present condition, the nanoparticles are unstable and susceptible to slow aggregation. Then a dissolution-recrystallization process for nanospheres takes place, and the more stable $La(OH)_3$ nanomultipods emerge with the reaction proceeding for 6 h. This intermediate product consists of a mixture of nanomultipods with 200 nm in length and some nanospheres, as presented in Fig. 9b. The corresponding XRD patterns shows a preferential growth of (1 1 0) plane in hexagonal $La(OH)_3$ crystals (Fig. 8b), which is in agreement with the HRTEM observation. Lanthanide hydroxide nanorods prepared in this work have a hexagonal crystal structure, and it clearly shows that the hexagonal $Ln(OH)_3$ has a highly anisotropic structure along the *c*-axis, as reported previously for the formation of $Ln(OH)_3$ nanowires and nanotubes [31]. At t = 12 and 24 h, the nanospheres disappear gradually and only the nanorods exist (Fig. 9c and d). The shape of the product is fairly uniform nanorods with an average length of 400 nm. In the corresponding XRD patterns, the diffraction peak of (1 1 0) plane is strongly strengthened compared with the other peaks (Fig. 8c and d). On the basis of the above analyses, it can be concluded that the morphological evolution from nanoparticles to nanorods can be expressed as a nucleation-dissolution-recrystallization-growth mechanism, and inherent crystal structure of seeds plays an important role in the formation of nanorods. The nucleation-dissolution-recrystallization-growth process has been observed in the synthesis of t-selenium nanotubes and ceria nanowires.

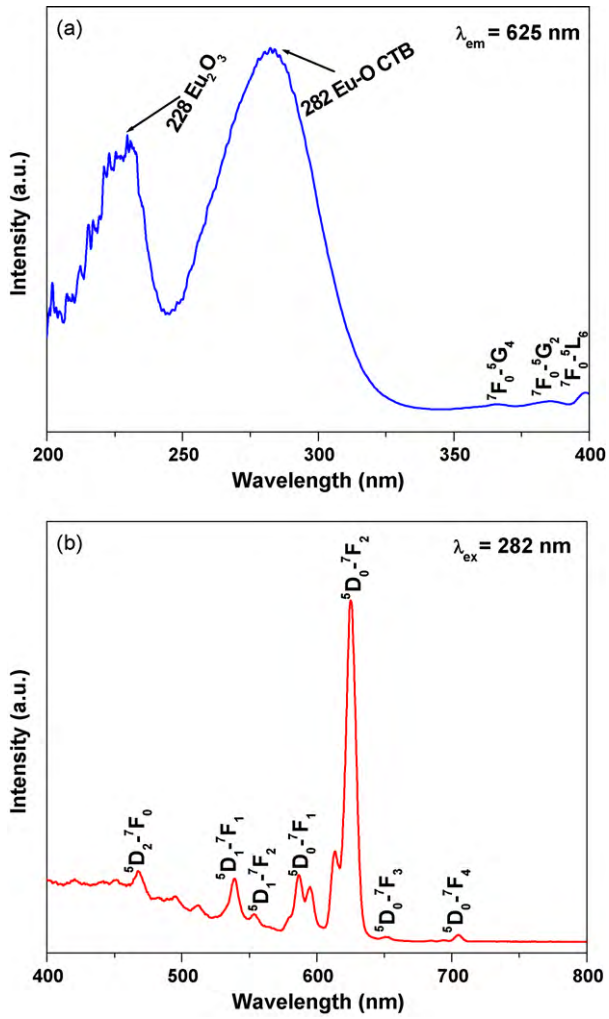

Fig. 6. Photoluminescence (a) excitation and (b) emission spectra of La_2O_3:Eu^{3+} nanorods.

The obtained experimental results are in agreement with those reported in the literatures [32,33]. Firstly, the colloidal $La(OH)_3$ nanoparticles were formed in the solution through a homogeneous nucleation process. When this colloidal dispersion was constantly hydrothermally treated at 150 °C, the small $La(OH)_3$ nanoparticles started to agglomerate as shown in Fig. 9a. Secondly, under the used hydrothermal conditions, the $La(OH)_3$ nanoparticles dissolved and recrystalized by increasing the hydrothermal treatment time. It was found that there were many protuberances on the surface of

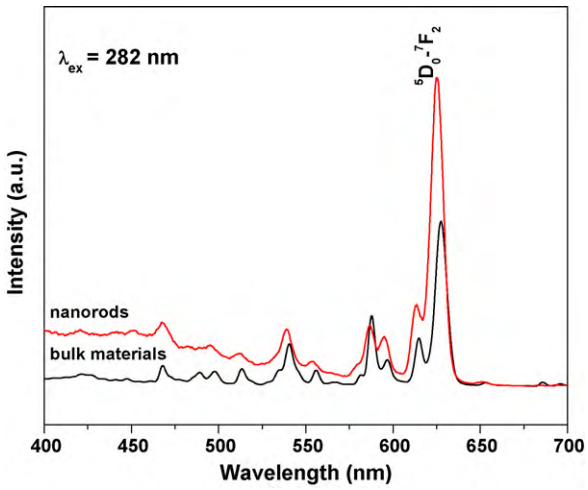

Fig. 7. Photoluminescence emission spectra of La_2O_3:Eu^{3+} nanorods under a excited wavelength of 282 nm, and the PL spectra of bulk sample is also given for comparison.

the nanoparticles (Fig. 9b), which provided many high-energy sites for nanocrystalline growth. So the dissolved $La(OH)_3$ in the solution might nucleate onto the small protuberances. Furthermore, there was an intrinsic tendency for the nucleation growth along the 1D direction due to the anisotropic crystal structure of the hexagonal $La(OH)_3$. The $La(OH)_3$ nanoparticles recrystallized into nanorods and grew until the $La(OH)_3$ nanoparticles were almost

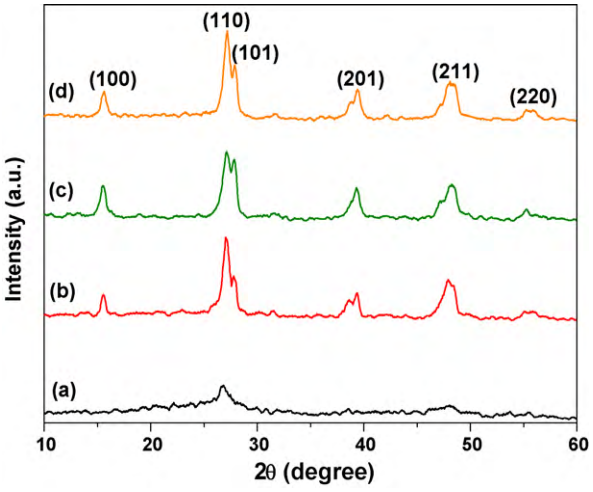

Fig. 8. XRD patterns of $La(OH)_3$ hydrothermally treated at 150 °C for (a) 1 h, (b) 6 h, (c) 12 h, and (d) 24 h.

Fig. 9. Schematic diagrams for the morphological evolution of $La(OH)_3$, together with the corresponding FE-SEM images: $La(OH)_3$ hydrothermally treated at 150 °C for (a) 1 h, (b) 6 h, (c) 12 h, and (d) 24 h.

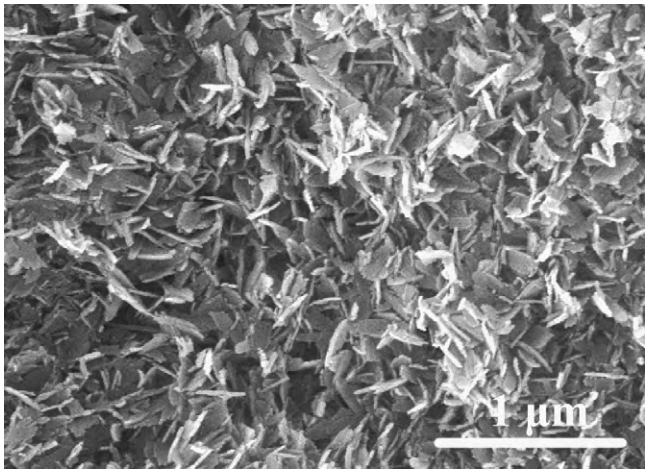

Fig. 10. FE-SEM images of $La(OH)_3$ nanodisks obtained without H_2O_2 in preparation system.

completely dissolved (Fig. 9c and d). A schematic representation of the $La(OH)_3$ nanostructure formation mechanism, at different steps, is illustrated in Fig. 9.

The use of H_2O_2 in the initial reaction solution is an external key factor in designing the morphologies of the final products. To determine the role of the H_2O_2 in the hydrothermal system, we carried out an additional blank experiment without H_2O_2, under similar hydrothermal conditions. The final products consist of the $La(OH)_3$ nanodisks with 10 nm and 200 nm in thickness and width, respectively (Fig. 10). In summary, there are two important key factors for determining the final shapes of $La(OH)_3$ nanocrystals. The first one is an intrinsic factor: the crystallographic phase of the nucleated seeds. The anisotropic structures of the thermodynamically stable hexagonal $La(OH)_3$ seeds induce anisotropic growth along their crystallographically directions. Therefore, the anisotropic shapes of nanocrystals are expected. The other external factor is the inorganic additive H_2O_2, which has a guiding effect on the morphology variations of the as-prepared nanostructured $La(OH)_3$ in the reaction system. When H_2O_2 was introduced to the preparation system, the $La(OH)_3$ nanorods were obtained. On the contrary, the nanodisk products were achieved under the similar conditions. It has been already demonstrated that the addition of simple inorganic compounds can influence the morphology of the products [34]. Other workers found that the simple ions direct the growth of nanoparticles into different shapes, highlighting the importance of these species [35,36]. H_2O_2 is a weak acid and can form H^+ and HO_2^- in solution. It is therefore reasonable to assume a similar effect of H_2O_2 on the produced morphologies. At the early stage of the reaction, due to the interaction between HO_2^- anions and La^{3+} cations, these anions can be selectively absorbed on specific facets of the initial $La(OH)_3$ crystals and change their surface energy. Furthermore, it leads directly to the different selective adsorption ability of NO_3^- and OH^- anions on the different crystal facets, consequently resulting in the different morphological evolutions of $La(OH)_3$ crystals. Therefore, the final adopted shape of $La(OH)_3$ products is the rodlike morphology. On the contrary, if H_2O_2 was not used, keeping identical all the other conditions, the nanodisk products were achieved under the same conditions. We speculate that the influences of additives (H_2O_2) on the growth of the $La(OH)_3$ crystals may include four aspects: influencing the interactions between NO_3^-, OH^- and HO_2^- anions and La^{3+} cations, affecting the adsorption of anions onto different crystal facets, changing the relative surface energy of the different crystal facets, and finally affecting the controlling growth mechanism. Although the morphological evolution process from nanoparticles to nanorods has been deduced, the intrinsic mechanism is not completely clear, further research on the morphological evolution mechanism and formation of the other 1D rare earth compounds is still in progress.

4. Conclusions

In summary, the uniform, dispersed and homogeneous $Ln(OH)_3$ and $La(OH)_3$:Eu^{3+} nanorods on a large-scale have been successfully prepared using a facile hydrothermal method free of any templates and catalysts. Following, the well-defined La_2O_3:Eu^{3+} nanorods were obtained by a subsequent heating treatment. The crystal structure, morphology, growth mechanism and optical properties of the products were characterized by means of XRD, FE-SEM, TEM, HRTEM, SAED and PL. The influences of inorganic additives and intrinsic structure on the shapes of $Ln(OH)_3$ nanostructures have been investigated in detail. The intrinsic hexagonal structure of $Ln(OH)_3$ and a variety of external factors account on the shape evolution of the products. In this work, H_2O_2 does not leave any impurity in the reaction system and makes the morphology to be modulated from the nanoparticles, nanomultipods to nanorods by increasing the reaction time. The formation mechanism for the $Ln(OH)_3$ 1D nanostructure have been proposed on a aggregation-dissolution-recrystallization procedure. It is meaningful to study the morphological evolution process of $Ln(OH)_3$ nanocrystals, which can be a systematic model and provide important information to the morphology-controllable synthesis of other rare earth compounds, and may be extended to the fields of crystal growth and design. The synthesized La_2O_3:Eu^{3+} nanorods achieved in this experiment exhibit a strong red emission corresponding to the $^5D_0 \rightarrow {}^7F_2$ transition (625 nm) of Eu^{3+} under UV excitation. The stronger emission and excellent dispersing property of La_2O_3:Eu^{3+} nanorods indicate that they potentially could be applied in the optical devices.

Acknowledgements

This project is financially supported by the National Natural Science Foundation of China (20701013 and 20801016) and the project of Heilongjiang Educational Department. Mr Liaohai Ge and Mrs Meiye Li are gratefully acknowledged for their help in the TEM and FE-SEM measurements.

References

[1] X.H. Huang, S. Neretina, M.A. Ei-Sayed, Adv. Mater. 21 (2009) 1880–4910.
[2] F. Boxberg, N. Søndergaard, H.Q. Xu, Nano Lett. 10 (2010) 1108–1112.
[3] L.W. Qian, Y.C. Gui, S.A. Guo, Q. Gong, X.F. Qian, J. Phys. Chem. Solids 70 (2009) 688–693.
[4] M. Mazloumi, N. Shahcheraghi, A. Kajbafvala, S. Zanganeh, A. Lak, M.S. Mohajerani, S.K. Sadrnezhaad, J. Alloys Compd. 473 (2009) 283–287.
[5] J.G. Deng, L. Zhang, C.T. Au, H.X. Dai, Mater. Lett. 63 (2009) 632–634.
[6] T.T. Yan, D.S. Zhang, L.Y. Shi, H.R. Li, J. Alloys Compd. 487 (2009) 483–488.
[7] Md.H. Zahir, T. Suzuki, Y. Fujishiro, M. Awano, J. Alloys Compd. 476 (2009) 335–340.
[8] G. Jia, Y.H. Zheng, K. Liu, Y.H. Song, H.P. You, H.J. Zhang, J. Phys. Chem. C 113 (2009) 153–158.
[9] M. Yang, H.P. You, K. Liu, Y.H. Zheng, N. Guo, H.J. Zhang, Inorg. Chem. 49 (2010) 4996–5002.
[10] L.W. Qian, W.M. Du, Q. Gong, X.F. Qian, Mater. Chem. Phys. 114 (2009) 479–484.
[11] H. Deng, C.M. Liu, S.H. Yang, S. Xiao, Z.K. Zhou, Q.Q. Wang, Cryst. Growth Des 8 (2008) 4432–4439.
[12] S. Mahapatra, G. Madras, T.N.G. Row, Ind. Eng. Chem. Res. 46 (2007) 1013–1017.
[13] G. Jia, H.P. You, M. Yang, L.H. Zhang, H.J. Zhang, J. Phys. Chem. C 113 (2009) 16638–16644.
[14] Z. Yang, Y.L. Wen, N. Sun, Y.F. Wang, Y. Huang, Z.H. Gao, Y. Tao, J. Alloys Compd. 489 (2010) L9–L12.
[15] S.J. Zeng, G.Z. Ren, Q.B. Yang, J. Alloys Compd. 493 (2010) 476–480.
[16] C.X. Li, J. Lin, J. Mater. Chem. (2010), doi:10.1039/c0jm00031k.
[17] F. Zhao, M. Yuan, W. Zhang, S. Gao, J. Am. Chem. Soc. 128 (2006) 11758–11759.
[18] S.C. Vanithakumari, K.K. Nanda, Adv. Mater. 21 (2009) 3581–3584.
[19] S. Guo, Z.B. Wu, H.Q. Wang, F. Dong, Catal. Commun. 10 (2009) 1766–1770.
[20] X. Wang, Y.D. Li, Angew. Chem. Int. Ed. 41 (2002) 4790–4793.

[21] M. Yada, M. Mihara, S. Mouri, M. Kuroki, T. Kijima, Adv. Mater. 14 (2002) 309–313.
[22] J. Yang, G.G. Li, C. Peng, C.X. Li, C.M. Zhang, Y. Fan, Z.H. Xu, Z.Y. Cheng, J. Lin, J. Solid State Chem. 183 (2010) 451–457.
[23] N. Li, K. Yanagisawa, N. Kumada, Cryst. Growth Des 9 (2009) 978–981.
[24] N. Zhang, R. Yi, L.B. Zhou, G.H. Gao, R.R. Shi, G.Z. Qiu, X.H. Liu, Mater. Chem. Phys. 114 (2009) 160–167.
[25] J. Yang, C.X. Li, Z.Y. Cheng, X.M. Zhang, Z.W. Quan, C.M. Zhang, J. Lin, J. Phys. Chem. C 111 (2007) 18148–18154.
[26] H.Q. Liu, L.L. Wang, W.Q. Huang, Z.W. Peng, Mater. Lett. 61 (2007) 1968–1970.
[27] Y. Tao, G.W. Zhao, X. Ju, X.G. Shao, W.P. Zhang, S.D. Xia, Mater. Lett. 28 (1996) 137–140.
[28] Z.G. Wei, L.D. Sun, C.S. Liao, C.H. Yan, S.H. Huang, Appl. Phys. Lett. 80 (2002) 1447–1449.
[29] Y.W. Jun, J.H. Lee, J.S. Choi, J. Cheon, J. Phys. Chem. B 109 (2005) 14795–14806.
[30] L.X. Liu, H.W. Song, Z.X. Liu, L.M. Yang, S.Z. Lu, Phys. Chem. Chem. Phys. 8 (2006) 303–308.
[31] X. Wang, Y.D. Li, Chem. Eur. J 9 (2003) 5627–5635.
[32] L. Yan, R.B. Yu, J. Chen, X.R. Xing, Cryst. Growth Des 8 (2008) 1474–1477.
[33] G.C. Xi, K. Xiong, Q.B. Zhao, R. Zhang, H.B. Zhang, Y.T. Qian, Cryst. Growth Des 6 (2006) 577–582.
[34] S.H. Im, Y.T. Lee, B. Wiley, Y.N. Xia, Angew. Chem. Int. Ed. 44 (2005) 2154–2157.
[35] J.Q. Hu, Q. Li, N.B. Wong, C.S. Lee, S.T. Lee, Chem. Mater. 14 (2002) 1216–1219.
[36] A. Filankembo, M.P. Pileni, J. Phys. Chem. B 104 (2000) 5865–5868.